Chemistry Research Journal, 2019, 4(6):135-150

Available online www.chemrj.org

Research Article

ISSN: 2455-8990
CODEN(USA): CRJHA5

Theoretical Study of Naphtho Aza Oxa Thia Crown Metal Ion Complexes: Deformation and NICS(0) Aromaticity

Roya Afsharpour, Esmael Rostami*

Department of Chemistry, Payame Noor University, PO BOX 19395-3697 Tehran, Iran.
Corresponding Author E-mail: Esmaelrostami@gmail.com

Abstract Naphthalene sulfide aza crown complex formation with metal ions (K^+, Na^+, Li^+, Ca^{2+}, Mg^{2+}, Sr^{2+}, Ag^+, Pb^{2+}, Cd^{2+}, Hg^{2+}, La^{3+}) was studied theoretically. The findings revealed that La^{3+} ion forms the most stable complex. The thermodynamic binding constants of metal ions and crown represented as follow: K^+< Ag^+<Na^+<Li^+<Sr^{2+}<Ca^{2+}<Pb^{2+}<Cd^{2+}<Hg^{2+}<Mg^{2+}<La^{3+}. The effect of complex formation on the NICS(0) aromaticity and deformation of aromatic rings were investigated and showed that more deformed rings have the higher NICS(0) aromaticity.

Keywords Bisnaphthosulfide aza oxa thia crown, macrocycle, La^{3+} ion, deformation, NICS(0) aromaticity

Introduction

Self-assembly constructs supramolecular systems via nonbonding interactions [1]. Nonbonding interactions form various systems via assembly of molecules and ions [2]. Construction of nano systems using molecules, atoms and small constituents (bottom up) is an example of the function of nonbonding interactions for generation of expanded structures [3]. On the other hand, numerous biological systems and life processes contain nonbonding interactions to form tissues in plants and animals and manage the processes in their bodies [4]. Complexation of metal ions with receptors is a significant procedure to selectively determine metal ions and molecules in a wide variety of samples [5]. These studies opened the gates of supramolecular chemistry [6], self-assembly [7], host-guest chemistry [8] and as a result the study of complicated structures such as biological systems and nanostructures [9].

Lanthanide ions are easy hydrolysable and have unique properties [10]. These properties make them as compatible and useful ions for biological systems [11]. Their complexes have been used as optical signal amplification [12], MRI contrast agents [13], imaging [14] and luminescent sensors [15]. Ligands with several donor atoms and well matched structure can stabilize lanthanide ions in aqueous media and especially in biological systems [16]. Based on the mentioned properties a series of analytical methods have been used to determine concentration of La^{3+} ion in various samples [17]. Theoretical methods with reliable procedures have significant advantages compared to experimental techniques such as environmental considerations, the use of more examples, lower costs, time saving and the same [18]. A variety of receptors have been employed to selective complex formation and determination of La^{3+} ion, such as crown ethers [19], aza crowns especially cyclen [20], podands [21], calixarenes [22], nanostructured structures [23], fluorescent receptors [24] and more.

Nucleus-independent chemical shift *(*NICS*)* is the most popular index to define aromatic character of rings in recent years [25]. By definition NICS is the negative anisotropic magnetic shielding at the center of ring [26]. Macrocycles

through complex formation undergo a series of reorganizations and deformations in their structure to form more stable complexes [27]. Thus, study and evaluation of aromatic ring deformations and aromaticity in this process is worthwhile for host-guest aggregation in a large number of systems [28].

In this research work theoretical study of complexation of a new bisnaphthosulfide aza oxa thia crown (lariate) bearing acetic acid with metal ions was investigated theoretically in gas phase.

Computational Methods

Gaussian 09 software package was used for optimization of crown and complexes [29]. GussView 5 was used to construct input files and evaluation of output results [30]. DFT b3lyp/6-31g and HF/Lanl2DZ basis sets and methods were used to optimization of crown (**1**). HF/Lanl2DZ level of theory was used to optimize complexes. Frequency calculations identify the optimized structures as energy minima without imaginary frequencies (NIMG=0). Optimization methods and frequency calculations have been used to calculate Physical properties. Formation constants were calculated using thermochemical data extracted from frequency output calculations. NICS (0) aromaticity were calculated for aromatic ring and the deformation of rings were compared to aromaticity.

Results and Discussion

Bisnaphthosulfide aza oxa thia crown (**1**) structure is showed in Figure 1 and was optimized using DFT B3LYP/6-31g and HF/Lanl2DZ basis sets and methods. HF/Lanl2DZ method was used to optimize complexes and their frequency calculations were performed using same basis set and procedure. The calculated physical properties are summarized in Table 1. Total energy and zero point energy (Ee+ZPE), dipole moments, frontier orbitals energies and figures (Highest occupied molecular orbital (HOMO) and lowest unoccupied molecular orbital (LUMO)) were extracted from output data. The hardness, polarizability and band gap were calculated according to the following equations.

Energy is an important factor for comparison of systems. According to the Table 1 and Figure 2, energy of crown and complexes decrease as follow: $\mathbf{1}^{\mathbf{a}} < Ag^{+} < Cd^{2+} < Hg^{2+} < Ca^{2+} < La^{3+} < Sr^{2+} < K^{+} < Li^{+} < Pb^{2+} < Mg^{2+} < Na^{+} < \mathbf{1}^{\mathbf{b}}$ (Table 1)**.** Energy of crown that calculated using HF/Lanl2DZ is higher than that of b3lyp/6-31g method.

Band gap is the difference between HOMO and LUMO orbitals (eq. 1). Molecule or complex with higher band gap are more stable and with lower band gap are less stable. Similar to energy that discussed in above，crown (**1**) that optimized using HF/Lanl2DZ has the highest band gap and the band gap of crown obtained from B3LYP/6-31g is the lowest. The band gap order is as follow: $\mathbf{1}^{\mathbf{a}} < Hg^{2+} < La^{3+} < Cd^{2+} < Sr^{2+} < Ca^{2+} < Pb^{2+} < Ag^{+} < K^{+} < Na^{+} < Mg^{2+} < Li^{+} < \mathbf{1}^{\mathbf{b}}$ (Table 1)**.**

$$\text{Band gap} = E_{LUMO} - E_{HOMO} \quad (1)$$

Based on the following equation，hardness (η) is computed using the ionization potential and electron affinity. The ionization potential and electron affinity could be acquired from the HOMO and LUMO energies.

$$\eta = (IP - EA)/2 = (E_{LUMO} - E_{HOMO})/2 \quad (2)$$

$$EA = -E_{LUMO} \quad IP = -E_{HOMO} \quad (3)$$

According to the Table 1, hardness arrangement of crown (**1**) and complexes change as the following: $\mathbf{1}^{\mathbf{a}} < Hg^{2+} < La^{3+} < Cd^{2+} < Sr^{2+} < Ca^{2+} < Pb^{2+} < Ag^{+} < K^{+} < Na^{+} < Mg^{2+} < Li^{+} < \mathbf{1}^{\mathbf{b}}$ (Table 1). Sequence of hardness and band gap is similar. Band gap and Hardness diagrams of **1** and its complexes showed in Figure 3. According to the equation 1 and 2 band gap is larger than hardness.

Polarizability of crown and complexes is calculated theoretically and shows the flexibility of molecule. Mean diagonal polarizability on the main axes was calculated as the polarizability.

$$\alpha = (1/3)\,(\alpha_{XX} + \alpha_{YY} + \alpha_{ZZ}) \quad (4)$$

Less stable molecules have the higher polarizabiliy and vice versa. According to the Table 1 the order of polarizability are as follow: $Mg^{2+} < \mathbf{1}^{\mathbf{a}} < Cd^{2+} < Hg^{2+} < Pb^{2+} < Ag^{+} < Ca^{2+} < Sr^{2+} < Na^{+} < Li^{+} < K^{+} < La^{3+} < \mathbf{1}^{\mathbf{b}}$. Thus, crown (**1**) has the highest polarizability (HF/Lanl2DZ) and **1**.Mg^{2+} has the lowest polarizability. As a result, according to the polarizability, **1** is the least stable and **1**. Mg^{2+} is the most stable molecule (Figure 4).

Dipole moment of **1** and its complexes reported in Table 1 and the corresponding diagram is appeared in Figure 5. It has been known that molecules with higher dipole moment are less stable than those molecules with lower dipole moment. The classification of dipole moment is according to the sequence: $\mathbf{1}^{b}$<Pb^{2+}<Hg^{2+}<$\mathbf{1}^{a}$<Mg^{2+}<Cd^{2+}<Li^{+}<Ag^{+}<Na^{+}<K^{+}<La^{3+}<Ca^{2+}<Sr^{2+}. Based on the dipole moment, **1**. Sr^{2+} complex has the highest dipole moment and thus is the least stable complex and **1** has the lowest dipole moment and is the most stable molecule.

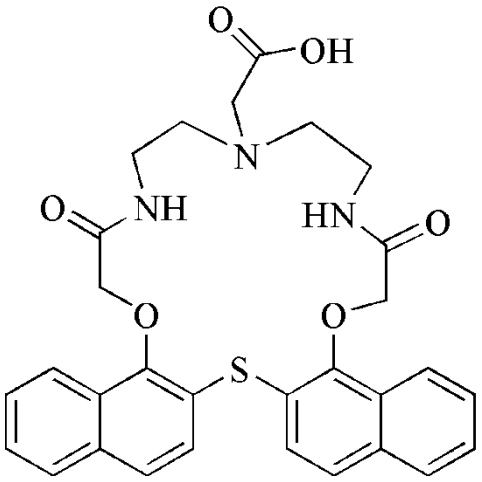

1

*Figure 1: Bisnaphthosulfide aza oxa thia Crown (**1**)*

Table 1: Calculated physical properties of crown (**1**) and complexes

	Entry[b]	Energy/A.U.[c]	E_{HOMO}/ev	E_{LUMO}/ev	Band Gap/ev	Hard.[d]	Dip./D.[e]	Polar.[f]
1	**1**[a]	-2173.356110	-0.20232	-0.04630	0.15602	0.07801	4.3974	176.211
2	**1**	-1774.233432	-0.29074	0.07295	0.36369	0.181845	3.6139	687.155
3	**1.Li^{+}**	-1781.610820	-0.39058	-0.04533	0.34525	0.172625	7.0649	267.721
4	**1.Na^{+}**	-1774.337655	-0.38991	-0.06435	0.32556	0.16278	8.8379	265.985
5	**1.K^{+}**	-1802.014558	-0.38743	-0.06938	0.31805	0.159025	10.6297	298.756
6	**1.Mg^{2+}**	-1774.713477	-0.48715	-0.15304	0.33411	0.167055	4.7331	145.960
7	**1.Ca^{2+}**	-1810.117159	-0.48761	-0.21089	0.27672	0.13836	10.9269	237.136
8	**1.Sr^{2+}**	-1804.011304	-0.48675	-0.21010	0.27665	0.138325	11.7811	239.522
9	**1.Ag^{+}**	-1918.996598	-0.39073	-0.07870	0.31203	0.156015	7.2713	225.802
10	**1.Pb^{2+}**	-1777.157765	-0.49114	-0.20934	0.2818	0.1409	3.7210	202.317
11	**1.Hg^{2+}**	-1815.101363	-0.48260	-0.24848	0.23412	0.11706	4.1294	197.187
12	**1.Cd^{2+}**	-1820.331321	-0.48688	-0.22970	0.25718	0.12859	5.9665	186.264
13	**1.La^{3+}**	-1804.323488	-0.58795	-0.33209	0.25586	0.12793	10.8983	304.899

a: DFT b3lyp/6-31g, b: HF/Lanl2DZ,c: Ee+ZPE, d: Hardness; e: Dipole moments (Debye); f: Polarizability

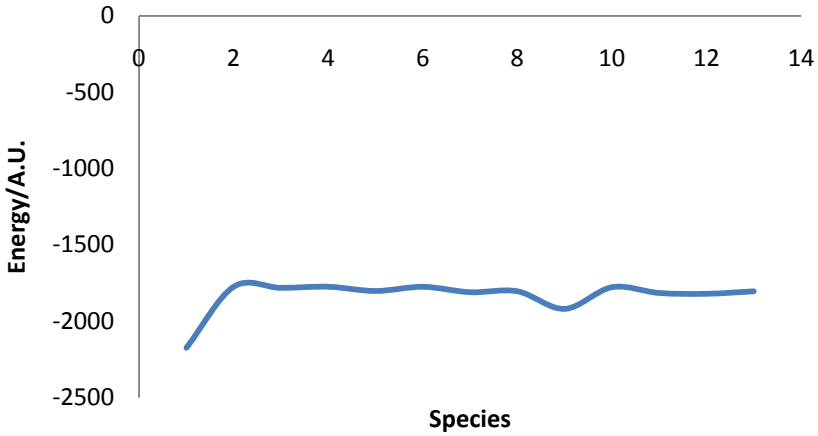

*Figure 2: Energy (Ee+ZPE) of crown (**1**) and complexes*

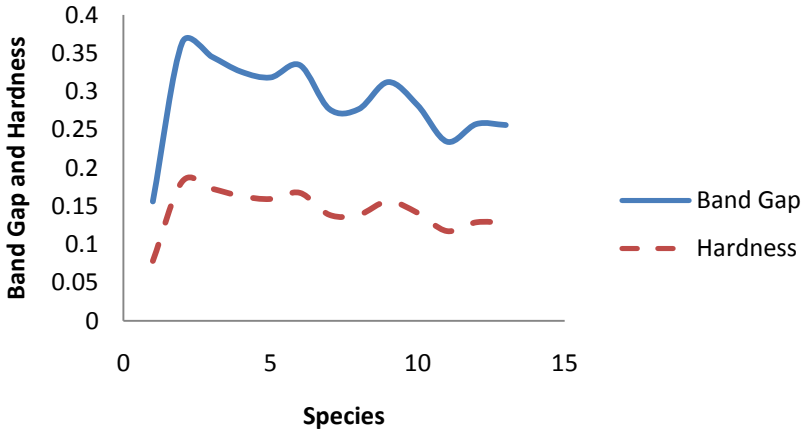

*Figure 3: Band Gap and Hardness of crown (**1**) and complexes.*

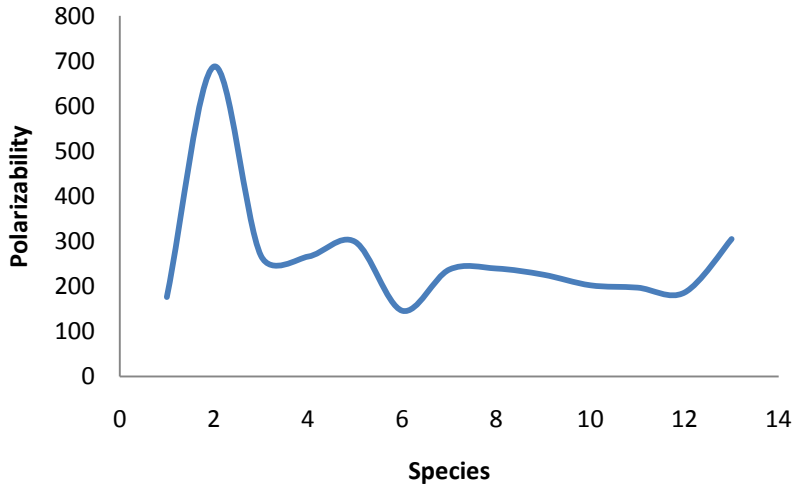

*Figure 4: Polarizability of crown (**1**) and complexes*

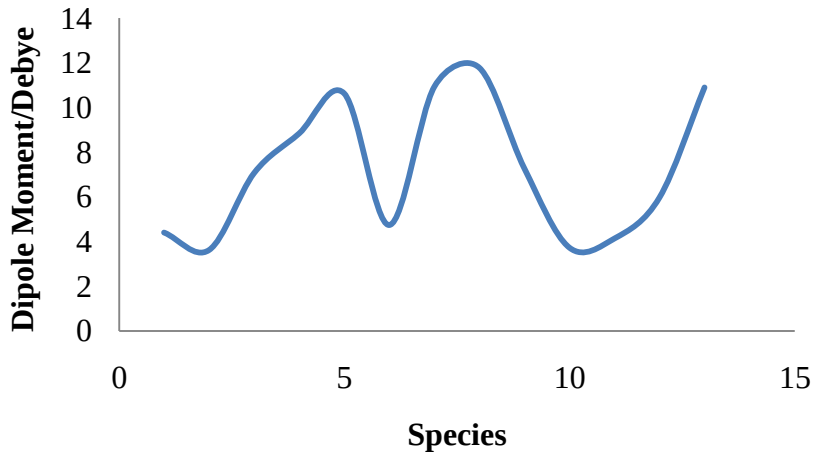

*Figure 5: Dipole moment of **1** and complexes*

Table 2: Calculated thermochemical properties (ΔH+ZPE and ΔG+ZPE) of **1** and its complexes.

Entry[a]	ΔH, Hartree/Part.	Hartree/Part. ΔG,	Entry[a]	ΔH, Hartree/Part.	ΔG, Hartree/Part.
1[b]	-2172.766036	-2172.87346	**1.La^{3+}**	-1803.691494	-1803.793546
1	-1773.603809	-1773.707455	**Li^{+}**	-7.233623	-7.248731
1.Li^{+}	-1780.977148	-1781.079094	**Na^{+}**	0.002360	-0.014429
1.Na^{+}	-1773.704866	-1773.809862	**K^{+}**	-27.703345	-27.720882
1.K^{+}	-1801.381929	-1801.489214	**Mg^{2+}**	0.002360	-0.014489
1.Mg^{2+}	-1774.078207	-1774.175032	**Ca^{2+}**	-35.607989	-35.625562
1.Ca^{2+}	-1809.483986	-1809.58493	**Sr^{2+}**	-29.539664	-29.558353
1.Sr^{2+}	-1803.378292	-1803.480902	**Ag^{+}**	-144.656780	-144.675746
1.Ag^{+}	-1918.363964	-1918.47029	**Pb^{2+}**	-2.5993	-2.6192
1.Pb^{2+}	-1776.524735	-1776.627507	**Hg^{2+}**	-40.4916	-40.5114
1.Hg^{2+}	-1814.468751	-1814.57171	**Cd^{2+}**	-45.723040	-45.742096
1.Cd^{2+}	-1819.698373	-1819.800574	**La^{3+}**	-29.535060	-29.554397

a: HF/Lanl2DZ, b: DFT b3lyp/6-31g

Table 3: Calculated thermochemical properties (ΔH+ZPE and ΔG+ZPE) of complex formation reactions.

Entry[a]	ΔΔH, Hartree/ Part.[b]	ΔΔG, Hartree/ Part.[c]	ΔΔH, Kcal/mol[d]	ΔΔG, Kcal/mol	K_f	Log K_f
1.Li^{+}	-0.139716	-0.122908	-87.673047	-77.125876	3.418×10^{56}	56.533
1.Na^{+}	-0.103417	-0.087978	-64.895098	-55.206986	2.931×10^{40}	40.467
1.K^{+}	-0.074775	-0.060877	-46.921985	-38.200865	1.003×10^{28}	28.001
1.Mg^{2+}	-0.476758	-0.453088	-299.169935	-284.316797	2.547×10^{208}	208.406
1.Ca^{2+}	-0.272188	-0.251913	-170.800419	-158.077674	7.447×10^{115}	115.871
1.Sr^{2+}	-0.234819	-0.215094	-147.351035	-134.973420	8.638×10^{98}	98.936
1.Ag^{+}	-0.103375	-0.087089	-64.868742	-54.649131	1.143×10^{40}	40.058
1.Pb^{2+}	-0.321626	-0.300852	-201.823209	-188.787337	2.411×10^{138}	138.382
1.Hg^{2+}	-0.373342	-0.352855	-234.275465	-221.419688	2.004×10^{162}	162.302
1.Cd^{2+}	-0.371524	-0.351023	-233.134653	-220.270091	2.880×10^{161}	161.459
1.La^{3+}	-0.552625	-0.531694	-346.777161	-333.642770	3.650×10^{244}	244.562

a: HF/Lanl2DZ, b: Hartree/Particle = 627.509 Kcal/mol, c: R = 1.98720 Cal/mol.K , d: T = 298.150 K

Based on the data reported in Table 2 and Table 3, formation constants of complexes are in the array of K^+< Ag^+<Na^+<Li^+< Sr^{2+}<Ca^{2+}<Pb^{2+}<Cd^{2+} <Hg^{2+}<Mg^{2+}<La^{3+}. The complexes of metal ions with two and three charges are more stable than complexes of metal ions with one equivalent charge. Complex formation between crown and metal ions depend on the several factors such as the size of crown ring and the radius of metal ion, charge of metal ion, solvent, three dimensional structure of crown and reorganization, acidity of medium, temperature and so on.
Optimized structure of crown (**1**) is appeared in Figure 6 from two sides. Optimized structure and atom numbering of **1**. La^{3+} complex from three sides was reported in Figure 7 and Figure 8. Based on these figures donor atoms and groups in complex formation with $La^{3+}$are two oxygen atoms and one aromatic ring.

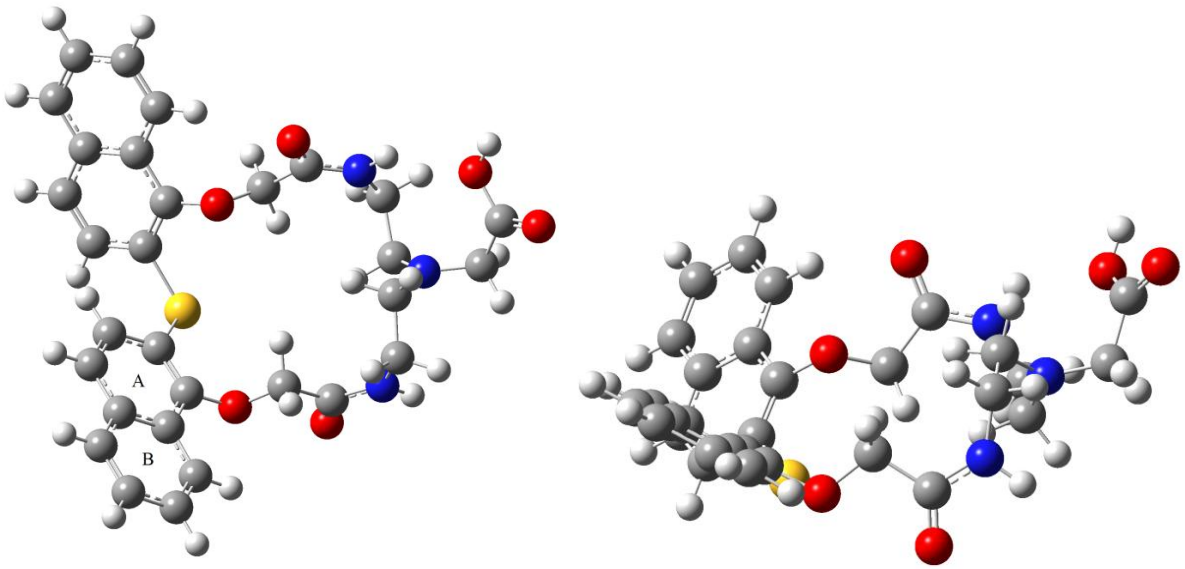

*Figure 6: The calculated 3D structure of crown (**1**) from two sides*

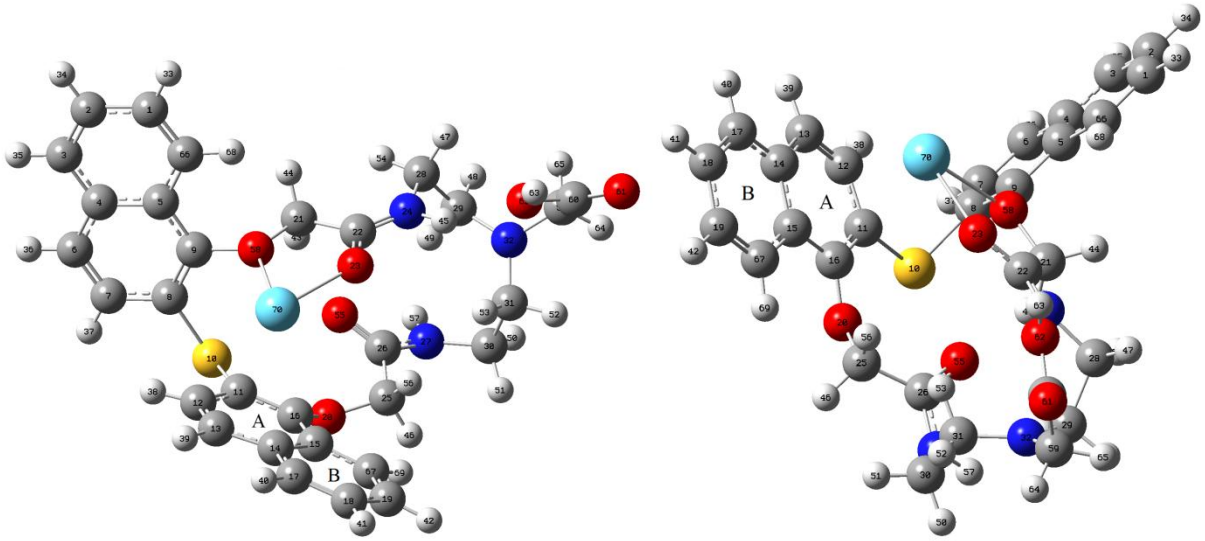

*Figure 7: The calculated 3D structure of **1**.La^{3+} complex from two sides.*

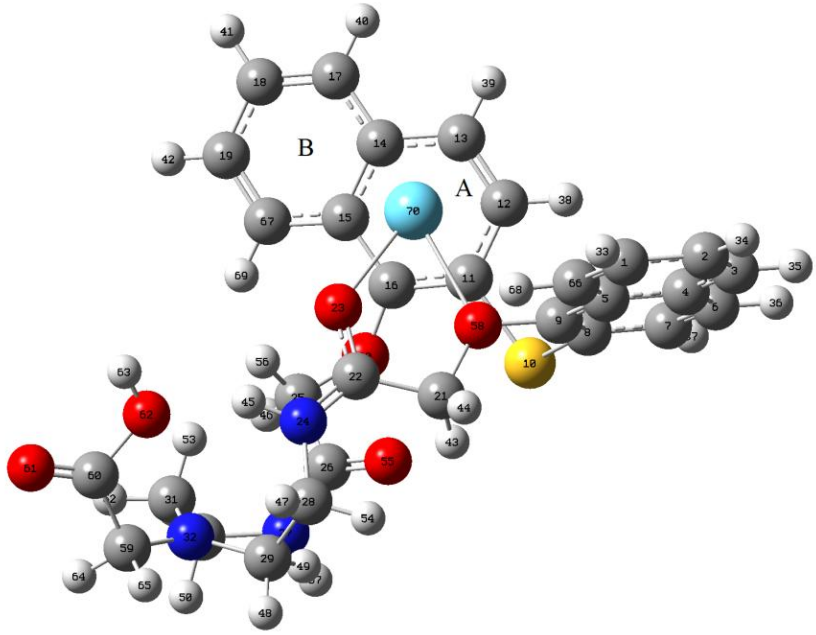

*Figure 8: The calculated 3D structure of **1**.La^{3+} complex from another side*

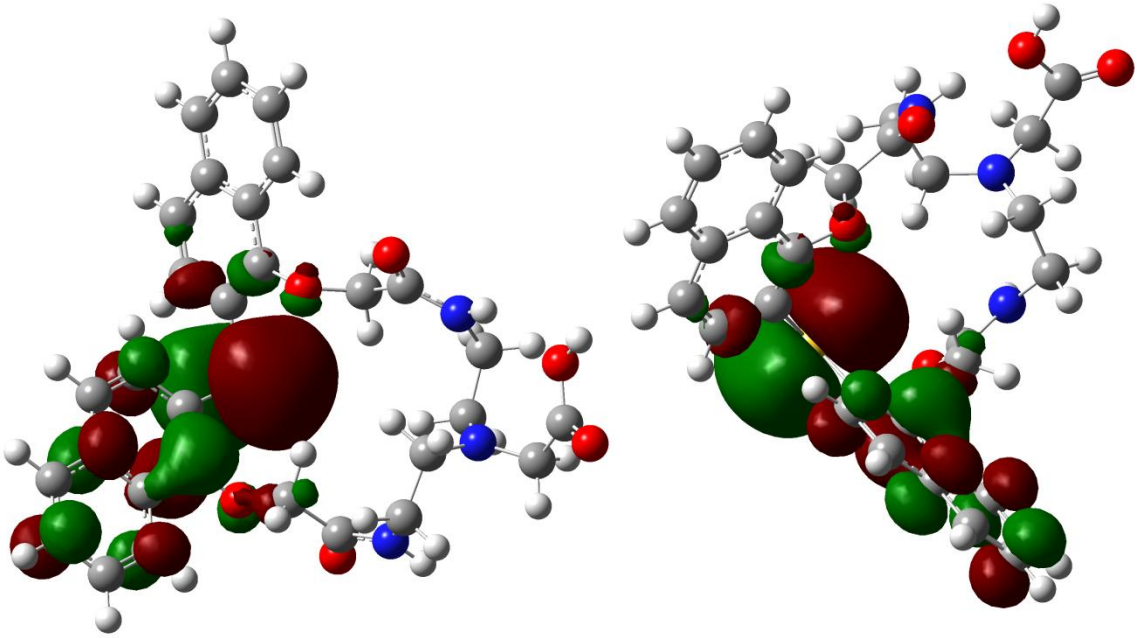

*Figure 9: HOMO orbital of crown (**1**) from two sides*

Electron distribution figures on the crown (**1**), using calculated HOMO and LUMO orbitals, was reported in Figure 9 and Figure 10. The HOMO orbital is distributed strongly over sulfur atom and moderately on one naphthalene ring. The LUMO orbital was distributed extensively on one naphthalene ring and weakly on another naphthalene ring.

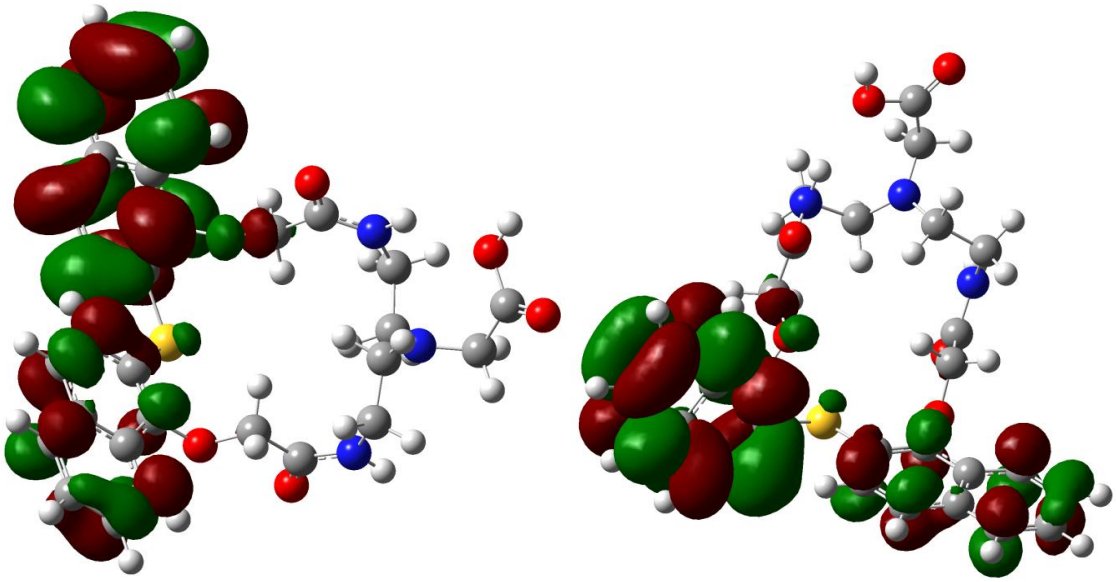

*Figure 10: LUMO orbital of crown (**1**) from two sides*

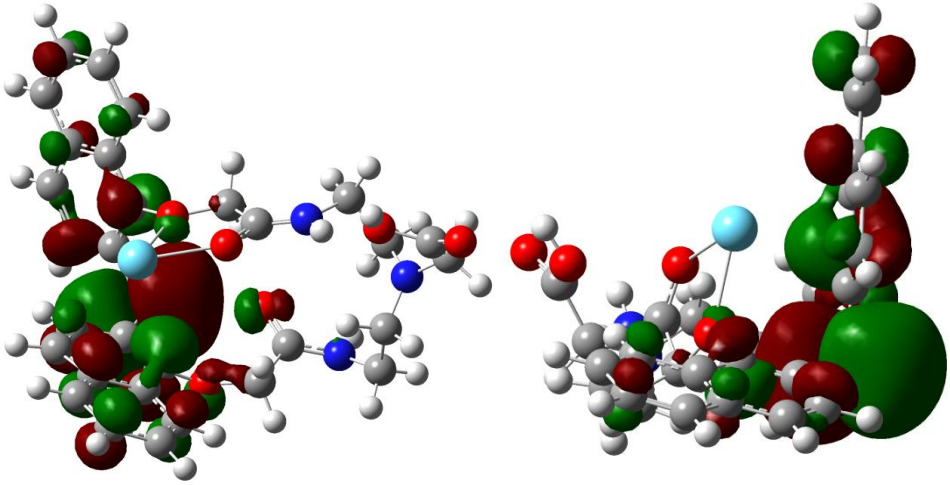

*Figure 11: HOMO orbital of **1**.La^{3+} complex from two sides*

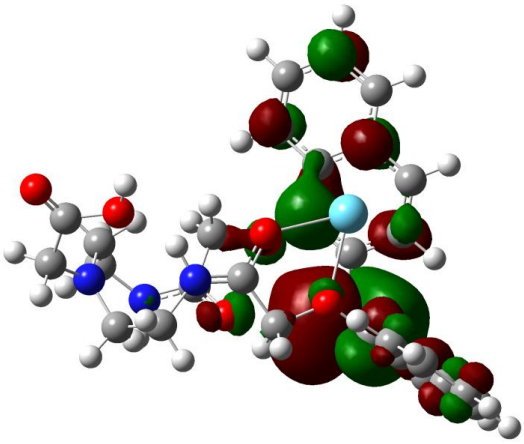

*Figure 12: HOMO orbital of **1**.La^{3+} complex from other side*

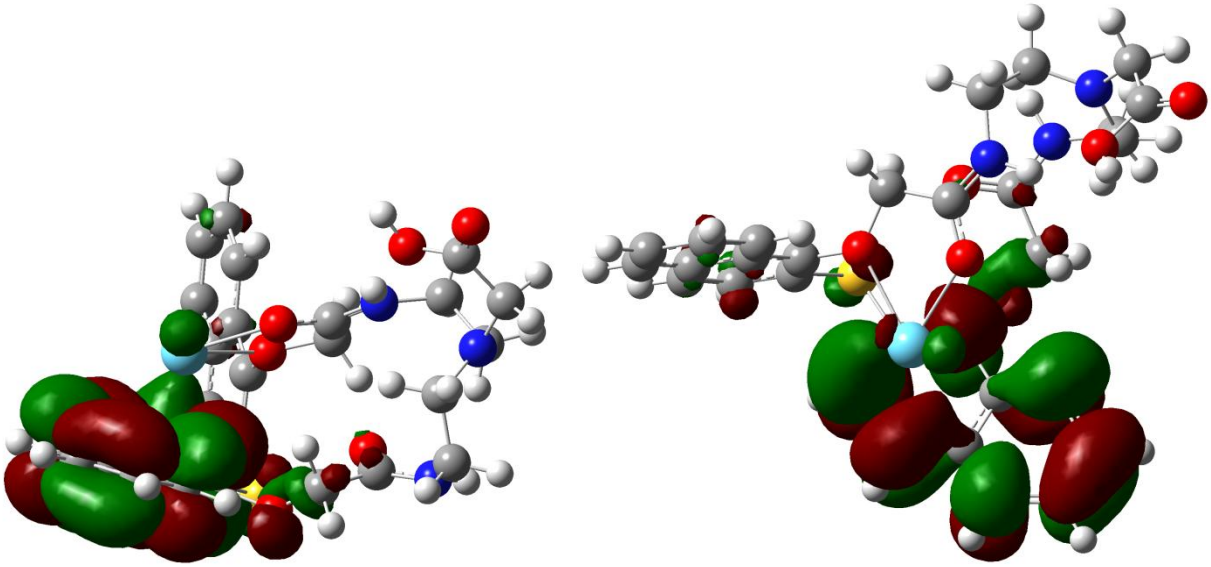

*Figure 13: LUMO orbital of **1**.La^{3+} complex from two sides.*

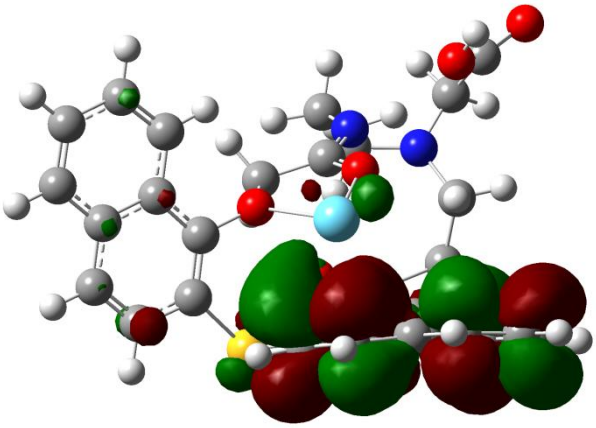

*Figure 14: LUMO orbital of **1**.La^{3+} complex from other side.*

HOMO orbital of **1**.La^{3+} complex was reported in Figure 11 and Figure 12. The HOMO orbital is distributed weakly on naphthalene rings and extensively on sulfur atom and La^{3+} isn't encountered. In HOMO orbital the interaction between La^{3+} ion and naphthalene ring is showed. Electron distribution on naphthalene ring is asymmetric (C16, q=0.443917, Table 4) and near the La^{3+} the carbon atom is positive because of electron transfer between carbon and La^{3+} (q=2.140753, Table 4). The LUMO orbital was distributed extensively on the pyridine ring and weakly on the sulfur atoms. Again, similar to HOMO orbital, the La^{3+} metal ion is bare (Figure 13 and Figure 14).

Charge Distribution

In order to give evidence on the reactive sites of the **1**.La^{3+} complex and predict the behavior of molecule, Mullikan charges distribution over the atoms were calculated (Table 4). The local valence electron density over atom i created from one molecular orbital is:

$$q_i = n\, c_i^2 \qquad (5)$$

where q_i is local valence electron density, n number of valence electrons represented in molecular orbital (MO) and c_i coefficient of MO orbital over the atom, i in the linear combination of atomic orbital (LCAO) representation.

As a result, Q_i the entire valence electron density over atom, i owning to overall molecular orbitals (MOs) is calculated using the following equation:

$$Q_i = \Sigma\, q_i \qquad (6)$$

According to the Table 4 positive and negative charges are distributed over the **1**.La^{3+} complex. The main intermolecular charge transfer between La^{3+} ion and C_{16} of aromatic ring was observed.

Table 4: Mullikan charges of **1**.La^{3+} complex

Atom	no	Charge	Atom	no	Charge	Atom	no	Charge
C	1	-0.191568	C	25	-0.167568	H	48	0.261575
C	2	-0.219216	C	26	0.520105	H	49	0.185661
C	3	-0.319034	N	27	-0.625820	H	50	0.254948
C	4	0.307434	C	28	-0.219585	H	51	0.210345
C	5	0.218286	C	29	-0.201400	H	52	0.239079
C	6	-0.354598	C	30	-0.235597	H	53	0.117199
C	7	-0.181761	C	31	-0.144102	H	54	0.212259
C	8	-0.586634	N	32	-0.457270	O	55	-0.495837
C	9	0.423487	H	33	0.254555	H	56	0.209783
S	10	0.680384	H	34	0.276082	H	57	0.404197
C	11	-0.861979	H	35	0.268324	O	58	-0.839815
C	12	-0.039385	H	36	0.280789	H	59	-0.310776
C	13	-0.428903	H	37	0.283927	H	60	0.500808
C	14	0.175832	H	38	0.340454	O	61	-0.310758
C	15	0.073385	H	39	0.324635	O	62	-0.731015
C	16	0.443917	H	40	0.276363	H	63	0.465356
C	17	-0.334831	H	41	0.291294	H	64	0.281315
C	18	-0.189197	H	42	0.284611	H	65	0.253804
C	19	-0.220190	H	43	0.364182	C	66	-0.346177
O	20	-0.521245	H	44	0.284559	C	67	-0.237821
C	21	-0.169133	H	45	0.516283	H	68	0.198207
C	22	0.661906	H	46	0.286182	H	69	0.257111
O	23	-0.799193	H	47	0.245956	La	70	2.140753
N	24	-0.534917						

Geometrical Parameters

Selected geometrical parameters for crown (**1**) and **1**.La^{3+} complex were reported in Table 5 and Table 6. Dihedral angels of ring A and ring B in crown (**1**) evaluated and deformation of ring A is higher than deformation of ring B. one reason for this phenomenon is large effect of crown ring on the geometry of ring A next to the crown ring (Figure 15). Ring B is far from the crown ring, thus this effect is smaller and deformation is lower. The same reason could be applied to explain similar results for **1**.La^{3+} complex in Figure 16. Also, in Figure 17 dihedral angels of ring A in crown (**1**) and **1**.La^{3+} complex were studied and deformation in complex is larger compared to deformation in crown (**1**) ring A. Similar results have been obtained by evaluation of ring B in crown (**1**) and complex and findings revealed that deformation in complex is larger than crown (**1**) (Figure 18).

Table 5: Selected bonds, angels and dihedral angels of crown (**1**)

Bond	Bond Lengh/Å	Angel	Angel size/deg	Dihedral Angel	Angel Size/deg
R(1,2)	1.4223	A(5,4,6)	119.1188	D(11,12,13,14)	-1.5664
R(1,66)	1.3709	A(4,6,7)	120.6241	D(12,13,14,15)	1.076
R(2,3)	1.3703	A(6,7,8)	120.821	D(13,14,15,16)	1.3712
R(3,4)	1.4239	A(7,8,9)	119.3073	D(14,15,16,11)	-3.4631
R(4,5)	1.415	A(5,9,8)	121.3362	D(12,11,16,15)	3.0164
R(5,66)	1.4258	A(3,4,5)	118.8602	D(16,11,12,13)	-0.4812
R(4,6)	1.4259	A(2,3,4)	120.5345	D(15,14,17,18)	-0.7439
R(5,9)	1.4299	A(1,2,3)	120.3676	D(14,17,18,19)	-0.5653

R(6,7)	1.3663	A(2,1,66)	120.5261	D(17,18,19,67)	0.8276
R(7,8)	1.4255	A(4,5,66)	119.8119	D(18,19,67,15)	0.2399
R(8,9)	1.3689	A(4,5,9)	118.7069	D(14,15,67,19)	-1.5452
R(8,10)	1.826	A(1,66,5)	119.882	D(17,14,15,67)	1.7826
R(10,11)	1.8386	A(8,10,11)	102.241	D(7,8,11,12)	-55.61569
R(22,23)	1.233	A(9,8,10)	121.6236	D(8,10,11,12)	18.4084
R(60,61)	1.2143	A(10,11,16)	118.1946	D(8,10,11,16)	-164.5547
R(60,62)	1.3628	A(13,14,17)	122.1421	D(8,9,11,16)	132.85541
R(26,55)	1.2263	A(16,15,67)	121.9677	D(10,11,16,20)	3.9078
R(9,58)	1.3858	A(3,4,6)	122.0201	D(10,8,9,58)	-0.2477
R(26,27)	1.3719	A(9,5,66)	121.4735	D(10,12,14,19)	-1.33842

Table 6: Selected bonds, angels and dihedral angels of **1**.La^{3+} complex

Bond	Bond Lengh	Angel	Angel size	Dihedral Angel	Angel Size
R(1,2)	1.423	A(5,4,6)	119.2859	D(11,12,13,14)	-3.23
R(1,66)	1.3724	A(4,6,7)	121.5218	D(12,13,14,15)	-4.0045
R(2,3)	1.3684	A(6,7,8)	120.4403	D(13,14,15,16)	4.7668
R(3,4)	1.4256	A(7,8,9)	118.2117	D(14,15,16,11)	1.6625
R(4,5)	1.4213	A(5,9,8)	123.295	D(12,11,16,15)	-8.7525
R(5,66)	1.4285	A(3,4,5)	119.1784	D(16,11,12,13)	9.699
R(4,6)	1.4191	A(2,3,4)	120.7552	D(15,14,17,18)	-1.7752
R(5,9)	1.4241	A(1,2,3)	120.0058	D(14,17,18,19)	-0.7389
R(6,7)	1.374	A(2,1,66)	120.8346	D(17,18,19,67)	1.5786
R(7,8)	1.4169	A(4,5,66)	119.0872	D(18,19,67,15)	0.1663
R(8,9)	1.3809	A(4,5,9)	117.1752	D(14,15,67,19)	-2.6398
R(8,10)	1.8401	A(1,66,5)	120.1372	D(17,14,15,67)	3.4236
R(10,11)	1.8347	A(6,7,37)	120.456	D(7,8,12,11)	139.77031
R(9,58)	1.4368	A(3,4,5)	119.1784	D(7,8,10,11)	-117.8433
R(22,23)	1.3129	A(9,5,66)	123.7374	D(8,10,11,12)	48.4524
R(22,24)	1.2876	A(1,2,34)	119.5293	D(70,12,13,14)	-68.26001
R(60,61)	1.2016	A(8,10,11)	99.9629	D(70,13,14,15)	-67.28285
R(60,62)	1.3916	A(9,58,70)	111.0675	D(8,9,11,16)	141.12238
R(62,63)	0.9603	A(23,70,58)	63.1295	D(13,30,17,40)	171.69198
R(24,45)	1.0129	A(23,22,24)	120.3477	D(6,36,3,35)	-179.40491
R(58,70)	2.3987	A(61,60,62)	119.99	D(58,9,65,68)	2.88513
R(23,70)	2.2893	A(22,23,70)	131.1978	D(20,16,67,69)	2.03396

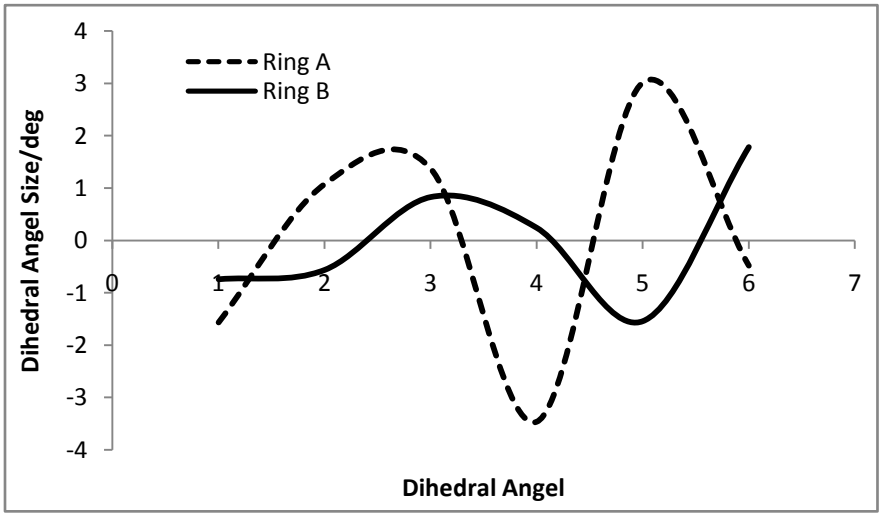

*Figure 15: Dihedral angels of ring A (dashed line) and ring B (solid line) in crown (**1**)*

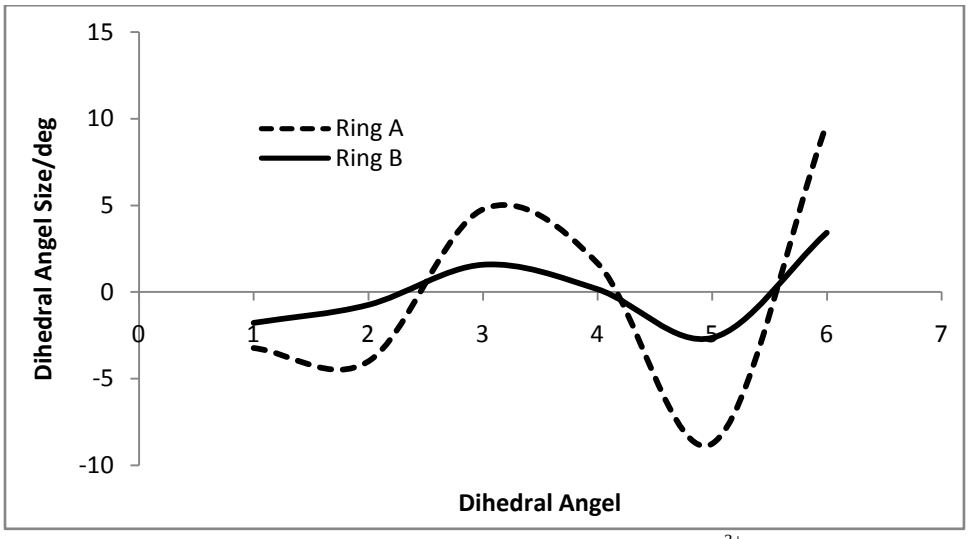

*Figure 16: Dihedral angels of ring A and ring B in **1**.La^{3+} complex.*

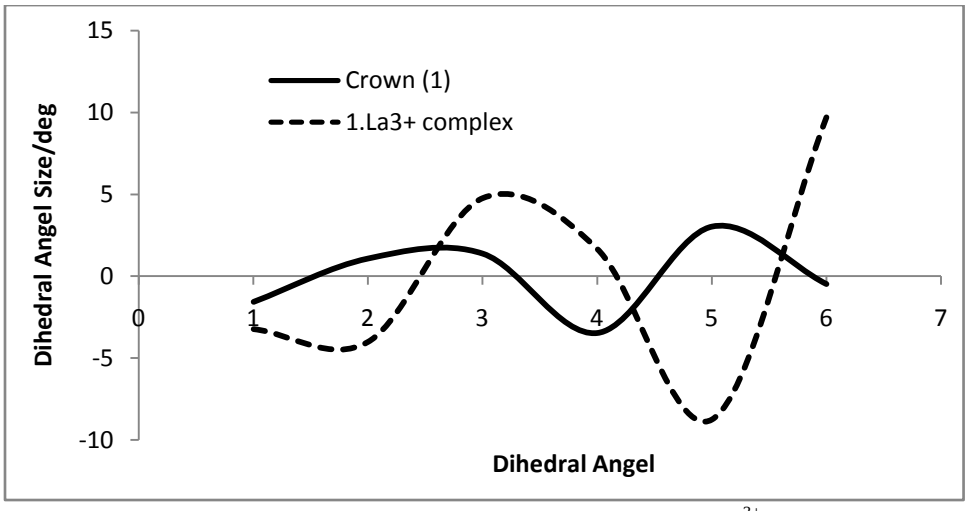

*Figure 17: Dihedral angels of ring A in crown (**1**) and **1**.La^{3+} complex.*

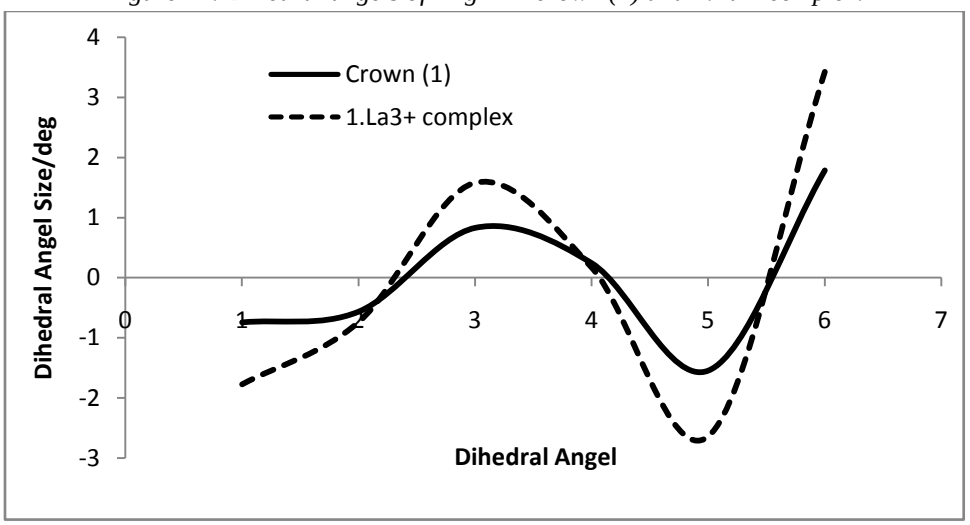

*Figure 18: Dihedral angels of ring B in crown (**1**) and **1**.La^{3+} complex*

Nucleus-independent chemical shifts *(*NICS*)* Studies

In order to defining the relationships between aromaticity and distortions of aromatic rings, aromaticity through Nucleus-independent chemical shifts (*NICS*) for naphthalene ring A and ring B in crown (**1**), complexes and free naphthalene were studied. The calculated NICS(0) and selected dihedral angels are appeared in Table 7. According to this data, ring A and ring B in crown (**1**) and nine metal ion complexes are aromatic, but, ring A in **1**.Hg^{2+} and **1**.Cd^{2+} complexes is nonaromatic (Figure 19). This is due to intensive interaction of Hg^{2+} and Cd^{2+} with ring A through covalent bond and formation of nonaromatic ring. Selected bonds, angels, dihedral angels and Milliken charges of **1**.Hg^{2+} and **1**.Cd^{2+} complexes were reported in Table 8. One naphthalene ring next to the metal ion in complexes has curvature and is not flat, due to the complex formation. Selected dihedral angels of naphthalene ring near the metal ion have been reported in Table 7. The data showed that D(13,14,15,67) and D(12,14,15,19) dihedral angels largely deviated from 180°, but D(17,14,15,16) and D(11,15,14,18) less deviated. These findings revealed that the naphthalene moiety is not smooth ring and have some curvature.

Table 7: NICS(0) and selected dihedral angels of crown (**1**), complexes and naphthalene

Row	Molecule	NICS(0)-A	NICS(0)-B	D(13,14,15,67)	D(12,14,15,19)	D(17,14,15,16)	D(11,15,14,18)
1	**Crown(1)**	-8.3486	-7.8101	-177.6057	-177.84056	-179.2405	178.74526
2	**1.Li^{+}**	-7.8507	-7.6563	-175.2102	-176.26172	-179.2505	178.63729
3	**1.Na^{+}**	-7.8920	-7.6270	-175.7087	-176.86960	-179.5882	178.89915
4	**1.K^{+}**	-8.0863	-7.6136	-176.31	-177.58013	-179.7965	179.27864
5	**1.Mg^{2+}**	-7.7393	-7.5935	-176.8222	-175.86335	-178.7026	176.84399
6	**1.Ca^{2+}**	-7.2878	-7.5040	-172.5048	-174.68595	179.9286	178.51594
7	**1.Sr^{2+}**	-7.6677	-7.5375	-173.1005	-175.41330	179.6218	178.84710
8	**1.Ag^{+}**	-7.4111	-7.6952	-175.8125	-176.64132	-179.7259	178.51682
9	**1.Pb^{2+}**	-8.8588	-7.7139	-173.4364	-175.59117	179.1741	178.54174
10	**1.Hg^{2+}**	-1.6432	-7.4378	-173.396	-169.91011	179.66	174.13174
11	**1.Cd^{2+}**	-4.2780	-7.7407	-172.8064	-172.39823	-179.6043	176.11346
12	**1.La^{3+}**	-9.0742	-7.4185	-170.8394	-174.07027	179.0298	178.97974
13	**Naphth.**	-7.5050	-7.5074				

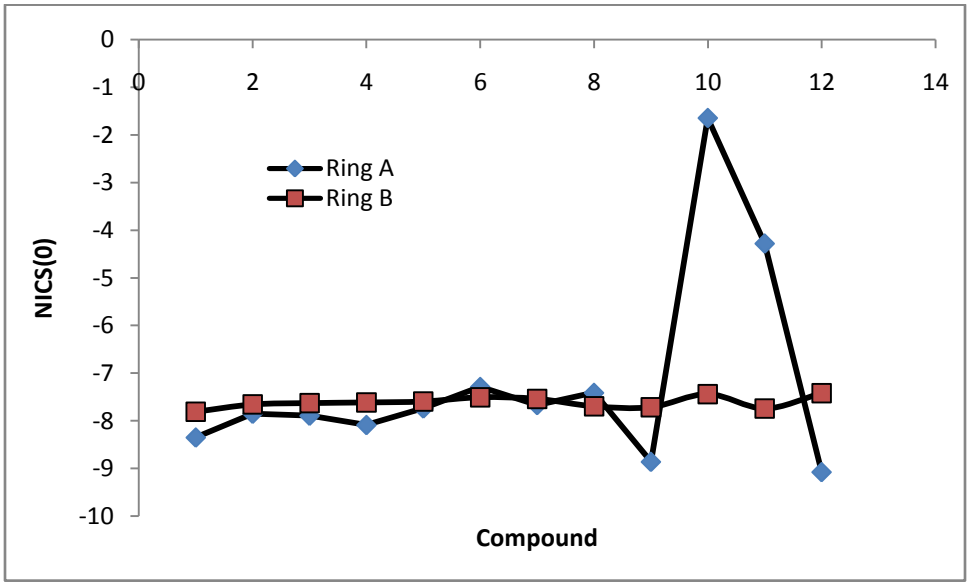

*Figure 19: NICS(0) of ring A and ring B in crown (**1**) and complexes*

Table 8: Selected bonds, angels, dihedral angels and Mullikan charges of **1**.Hg^{2+} and **1**.Cd^{2+}.

1.Hg^{2+} complex				**1**.Cd^{2+} complex			
Bond	**Bond/Å**	**Atom**	**Charge**	**Bond**	**Bond/Å**	**Atom**	**Charge**
R(11,12)	1.4016	C11	-0.554345	R(11,12)	1.4294	C11	-0.58322
R(12,13)	1.4268	C12	-0.046205	R(12,13)	1.4006	C12	-0.17627
R(13,14)	1.4571	C13	-0.584442	R(13,14)	1.4362	C13	-0.49141
R(14,15)	1.4196	C14	0.352319	R(14,15)	1.4215	C14	0.30063
R(15,16)	1.441	C15	0.059323	R(15,16)	1.4408	C15	0.09904
R(14,17)	1.412	C16	0.491766	R(14,17)	1.4196	C16	0.44653
R(17,18)	1.3765	C17	-0.348873	R(17,18)	1.3712	C17	-0.33796
R(18,19)	1.4161	C18	-0.183893	R(18,19)	1.4196	C18	-0.20049
R(19,67)	1.3729	C19	-0.235683	R(19,67)	1.3721	C19	-0.22049
R(12,70)	2.60857	C67	-0.235915	R(12,70)	2.44157	C67	-0.25287
R(13,70)	2.35546	S10	0.585059	R(13,70)	2.52607	S10	0.588071
R(10,11)	1.8239	Hg70	1.118658	R(10,11)	1.8256	Cd70	1.28162

Acknowledgement

The financial support of this work by Payame Noor University (PNU) Research Council is acknowledged.

References

[1]. Gunnlaugsson, T., (2016). Supramolecular pathways: Accessible self-assembly, *Nat. chem.* 8: 6.

[2]. Bai, Y., Luo, Q., Liu, J., (2016). Protein self-assembly via supramolecular strategies, *Chem. Soc. Rev.* 45: 2756-2767.

[3]. Lv, J., Hou, K., Ding, D., Wang, D., Han, B., Gao, X., Zhao, M., Shi, L., Guo, J., Zheng, Y., Zhang, X., (2017). Gold Nanowire Chiral Ultrathin Films with Ultrastrong and Broadband Optical Activity, *Angew. Chem.*56: 5055-5060.

[4]. Zhou, J., Du, X., Gao, Y., Shi, J., Xu, B., (2014). Aromatic–aromatic interactions enhance interfiber contacts for enzymatic formation of a spontaneously aligned supramolecular hydrogel, *J. Am. Chem. Soc.* 136:2970-2973.

[5]. Bhowmik, S., Ghosh, B.N., Marjomäki, V., Rissanen, K., (2014). Nanomolar pyrophosphate detection in water and in a self-assembled hydrogel of a simple terpyridine-Zn^{2+} complex, *J. Am. Chem. Soc.* 136:5543-5546.

[6]. Lehn, J. M., (2017). Supramolecular chemistry: Where from? Where to?, *Chem. Soc. Rev.* 46:2378-2379.

[7]. Wang, J., Liu, K., Xing, R., Yan, X., (2016). Peptide self-assembly: thermodynamics and kinetics, *Chem. Soc. Rev.* 45:5589-5604.

[8]. Yeung, M. C., Yam, V.W., (2015). Luminescent cation sensors: from host–guest chemistry, supramolecular chemistry to reaction-based mechanisms, *Chem. Soc. Rev.*44:4192-4202.

[9]. Collin, S., (2014). Nanostructure arrays in free-space: optical properties and applications, *Rep. Prog. Phys.* 77:126402.

[10]. Yang, D., Hou, Z., Cheng, Z., Li, C., Lin, J., (2015). Current advances in lanthanide ion (Ln^{3+})-based upconversion nanomaterials for drug delivery, *Chem. Soc. Rev.* 44:1416-1448.

[11]. Saio, T., Inagaki, F., (2016). NMR Structural Biology Using Paramagnetic Lanthanide Probe, Adv. Methods Struct. Biol., Springer, Tokyo, 315-340.

[12]. Ye, H., Li, Z., Peng, Y., Wang, C.C.,T. Li, Y., Zheng, Y.X., Sapelkin, A., Adamopoulos, G., Hernández, I., Wyatt, P.B., Gillin, (2014). Organo-erbium systems for optical amplification at telecommunications wavelengths, NatW.P., *Mat.* 13:382.

[13]. Zeng, J., Jing, L., Hou, Y., Jiao, M., Qiao, R., Jia, Q., Liu, C., Fang, F., Lei, H., Gao, M., (2014). Anchoring group effects of surface ligands on magnetic properties of Fe_3O_4 nanoparticles: towards high performance MRI contrast agents, *Adv. Mat.* 26:2694-2698.

[14]. Alcaraz, N., Boyd, B.J., (2017). Cubosomes as Carriers for MRI Contrast Agents, *Curr. Med. Chem.* 24:470-482.

[15]. Silvi, S., Credi, A., (2015). Luminescent sensors based on quantum dot–molecule conjugates, *Chem. Soc. Rev.* 44: 4275-4289.

[16]. Wada, H., Ooka, S., Yamamura, T., Kajiwara, T., (2016). Light Lanthanide Complexes with Crown Ether and Its Aza Derivative Which Show Slow Magnetic Relaxation Behaviors, *Inorg. Chem.* 56:147-155.

[17]. Pandya, A., Joshi, K.V., Sutariya, P.G. and Menon, S.K., (2012). Thioctic acid modified gold nanoparticles for highly specific and ultrasensitive detection of lanthanum in soil and water. *Anal. Methods*, 4: 3102-3106.

[18]. Evans, J.D., Jelfs, K.E., Day, G.M. and Doonan, C.J., (2017). Application of computational methods to the design and characterisation of porous molecular materials. *Chem. Soc. Rev.*, 46: 3286-3301.

[19]. Egorova, B.V., Oshchepkov, M.S., Fedorov, Y.V., Fedorova, O.A., Budylin, G.S., Shirshin, E.A. and Kalmykov, S.N., (2016). Complexation of Bi3+, Ac3+, Y3+, Lu3+, La3+ and Eu3+ with benzo-diaza-crown ether with carboxylic pendant arms. *Radiochim. Acta*, 104: 555-565.

[20]. Wilson, J.J., Birnbaum, E.R., Batista, E.R., Martin, R.L. and John, K.D., (2014). Synthesis and characterization of nitrogen-rich macrocyclic ligands and an investigation of their coordination chemistry with lanthanum (III). *Inorg.Chem.*, 54: 97-109.

[21]. Xu, W., Zhou, Y., Huang, D., Su, M., Wang, K., Xiang, M. and Hong, M., (2015). Luminescent sensing profiles based on anion-responsive lanthanide (III) quinolinecarboxylate materials: solid-state structures, photophysical properties, and anionic species recognition. *J. Mater. Chem. C*, 3: 2003-2015.

[22]. Hong, G., Wang, M., Li, X., Shen, L., Wang, X., Zhu, M. and Hsiao, B.S., (2015). Micro-nano structure nanofibrous p-sulfonatocalix [8] arene complex membranes for highly efficient and selective adsorption of lanthanum (III) ions in aqueous solution. *RSC Adv.*, 5: 21178-21188.

[23]. Dong, H., Du, S.R., Zheng, X.Y., Lyu, G.M., Sun, L.D., Li, L.D., Zhang, P.Z., Zhang, C. and Yan, C.H., (2015). Lanthanide nanoparticles: from design toward bioimaging and therapy. *Chem.Rev.*, 115: 10725-10815.

[24]. Areti, S., Bandaru, S., Teotia, R. and Rao, C.P., (2015). Water-Soluble 8-Hydroxyquinoline Conjugate of Amino-Glucose as Receptor for La3+ in HEPES Buffer, on Whatman Cellulose Paper and in Living Cells. *Anal.Chem.*, 87: 12348-12354.

[25]. Das, R. and Chattaraj, P.K., (2014). Guest–host interaction in an aza crown analog. *Int. J. Quantum Chem.*, 114: 708-719.

[26]. Zdetsis, A.D. and Economou, E.N., (2015). A Pedestrian Approach to the Aromaticity of Graphene and Nanographene: Significance of Huckel's (4 n+ 2) π Electron Rule. *J. Phys. Chem. C*, 119: 16991-17003.

[27]. Zhang, H. and Dearden, D.V., (1992). The gas-phase macrocyclic effect: reaction rates for crown ethers and the corresponding glymes with alkali metal cations. *J. Am. Chem. Soc.*, 114: 2754-2755.

[28]. Schleyer, P.V.R., Kiran, B., Simion, D.V. and Sorensen, T.S., (2000). Does Cr (CO) 3 complexation reduce the aromaticity of benzene? *J. Am. Chem. Soc.*, 122: 510-513.

[29]. Gaussian 09, Revision E.01, Frisch, M.J., Trucks, G.W., Schlegel, H. B., Scuseria, G. E., Robb, M.A., Cheeseman, J.R., Scalmani, G., Barone, V., Mennucci, B., Petersson, G.A., Nakatsuji, H., Caricato, M., Li, X., Hratchian, H.P., Izmaylov, A.F., Bloino, J., Zheng, G., Sonnenberg, J.L., Hada, M., Ehara, M., Toyota, K., Fukuda, R., Hasegawa, J., Ishida, M., Nakajima, T., Honda, Y., Kitao, O., Nakai, H., Vreven, T., Montgomery, Jr, J.A., Peralta, J.E., Ogliaro, F., Bearpark, M., Heyd, J.J., Brothers, E., Kudin, K.N., Staroverov, V.N., Kobayashi, R., Normand, J., Raghavachari, K., Rendell, A., Burant, J.C., Iyengar, S.S., Tomasi, J., Cossi, M., Rega, N., Millam, J.M., Klene, M., Knox, J.E., Cross, J.B., Bakken, V., Adamo, C., Jaramillo, J., Gomperts, R., Stratmann, R.E., Yazyev, O., Austin, A.J., Cammi, R., Pomelli, C., Ochterski,

J.W., Martin, R.L., Morokuma, K., Zakrzewski, V.G., Voth, G.A., Salvador, P., Dannenberg, J.J., Dapprich, S., Daniels, A.D., Farkas, Ö., Foresman, J.B., Ortiz, J. V., Cioslowski, J., and Fox, D.J., Gaussian, Inc., Wallingford CT, 2009.

[30]. Gauss View, Version 5, Dennington, R., Keith, T., Millam, J., *Semichem Inc.*, Shawnee Mission, KS, 2009.